No. 682 **March 2025**

A geometric multigrid solver for the incompressible Navier-Stokes equations using discretely divergence-free finite elements in 3D

C. Lohmann

ISSN: 2190-1767

A geometric multigrid solver for the incompressible Navier-Stokes equations using discretely divergence-free finite elements in 3D

Christoph Lohmann

March 24, 2025

Abstract

A geometric multigrid solution technique for the incompressible Navier-Stokes equations in three dimensions is presented, utilizing the concept of discretely divergence-free finite elements without requiring the explicit construction of a basis on each mesh level. For this purpose, functions are constructed in an a priori manner spanning the subspace of discretely divergence-free functions for the Rannacher-Turek finite element pair under consideration. Compared to mixed formulations, this approach yields smaller system matrices with no saddle point structure. This prevents the use of complex Schur complement solution techniques and more general preconditioners can be employed.

While constructing a basis for discretely divergence-free finite elements may pose significant challenges and its use prevents a structured assembly routine, a basis is utilized only on the coarsest mesh level of the multigrid algorithm. On finer grids, this information is extrapolated to prescribe boundary conditions efficiently. Here, special attention is required for geometries introducing bifurcations in the flow. In such cases, so called 'global' functions with an extended support are defined, which can be used to prescribe the net flux through different branches.

Various numerical examples for meshes with different shapes and boundary conditions illustrate the strengths, limitations, and future challenges of this solution concept.

Keywords. incompressible Navier-stokes equations; discretely divergence-free finite elements; geometric multigrid solver; three-dimensional space

1 Introduction

In this paper, we explore the concept of discretely divergence-free finite elements (DDFFE) in three dimensions for the Rannacher-Turek finite element pair to solve the incompressible Navier-Stokes equations. The framework is based on the idea of first eliminating the pressure unknowns in an a priori manner before discretization. As a result, the total number of degrees of freedom is significantly reduced compared to the mixed formulation and system matrices no longer have a saddle point structure, providing the possibility to use more general

preconditioners in multigrid solution techniques. This makes the approach more flexible and robust, especially when dealing with high anisotropies in the computational mesh or differential operators. However, these advantages come at the cost of the resulting system matrix for the steady Stokes equations behaving like a biharmonic operator, with a condition number of $\mathcal{O}(h^{-4})$ (cf. [Dör90; Tur94a]).

The idea of DDFFE dates back to the late 1970s and was initially studied for two-dimensional problems in [Cro76; Tem77; GM79; Gri79; Gri81; For81; Tho81]. While these publications primarily focus on the construction of basis functions for different discretization techniques, only a few references have addressed the development of efficient solution strategies. For instance, Dörfler [Dör90] and Verfürth [Ver89] introduced hierarchical preconditioning techniques that significantly reduce the condition number of the system matrices. Additionally, Turek [Tur91; Tur94a; Tur94b] developed efficient multigrid algorithms for the Crouzeix-Raviart [CR73] and Rannacher-Turek [RT92] finite element pairs, leading to mesh-independent convergence rates.

In three dimensions, discretely divergence-free finite elements were first studied in [Hec81; Gri81; For81; Tho81; CSS86], mainly focusing on simply connected domains with Dirichlet boundary conditions everywhere. More complicated problems, including doughnut-shaped domains or Neumann boundary conditions, were excluded due to the inherently more complicated task of constructing a basis in 3D. Furthermore, the design of efficient solution strategies was out of the scope of these references, making the approach less relevant for practical applications.

With this paper, we aim to fill this gap and shed new light on the use of discretely divergence-free finite elements in three dimensions. To this end, we extend the concept to more general meshes and design geometric multigrid solvers that do not require an explicit basis on finer mesh levels. On the coarsest level, we introduce a constructional characterization of a basis, which is particularly useful for designing interpolation operators by marching over a set of faces and associated edges. Although several design criteria are summarized, the explicit definition of an algorithm that generates such a basis is left undefined. For geometries introducing bifurcations in the flow, additional functions with an extended support are defined. The influence of these functions can be mimicked using so called "projection methods" without hindering the convergence behavior of the proposed multigrid algorithm.

To keep things simple, here we mainly focus on sample domains and outline several design criteria for the construction of a basis. The approach presented below is also restricted to numerical solutions, which do not exhibit non-vanishing net fluxes on closed boundary parts of the domain. This restriction ensures that sinks or sources do not exist within holes of the computational domain. Furthermore, we assume that the family of triangulations consists solely of meshes with planar faces. This assumption is crucial for the three-dimensional Rannacher-Turek FE pair to guarantee the optimal convergence of the scheme and to simplify the explicit construction of a spanning set for the space of discretely divergence-free finite elements. For other finite element pairs, such as the so called "Q_2-P_1" FE pair, which will be investigated in the future, these requirements might not be mandatory and can be avoided using similar techniques.

The remainder of this article is structured as follows: In the following section, we describe the concept of discretely divergence-free finite elements for the Rannacher-Turek finite element

Table 1: Value of Euler characteristics χ_v and χ_s for different types of three-dimensional volume and surface meshes, respectively.

χ_v	volume mesh
1	simply connected mesh
2	mesh with single hole
0	doughnut-shaped mesh

χ_s	surface mesh
2	closed convex polyhedron's surface
0	torus
1	simply connected two-dimensional mesh
0	two-dimensional mesh with one hole

space in three-dimensions. Special attention is given to the construction of a basis and the proper enforcement of boundary conditions, facilitating the application of direct numerical solution techniques for general geometries. Section 3 is dedicated to the construction of efficient multigrid solvers, which rely solely on the knowledge of a set of basis functions on the coarsest grid level. Especially, we introduce a prolongation operator that can be efficiently applied and preserves globally linear functions. Additionally, the treatment of boundary conditions is addressed in the absence of an explicitly known basis. The performance of the proposed multigrid algorithm is investigated in Section 4, where test problems with different geometries are considered. Finally, Section 5 provides a summary of the main findings and concluding remarks.

2 Discretely divergence-free finite elements

Let Ω be an open, bounded, and connected subdomain of $\mathbb{R}^3$ while $\mathcal{T}_h$ is a triangulation of Ω consisting of C_v hexahedral cells, F_v faces, E_v edges, and V_v vertices. Then the (volumetric) Euler characteristic of $\mathcal{T}_h$ is defined by

$$\chi_v = V_v - E_v + F_v - C_v,$$

which is is a toplogical invariant describing the topological space of Ω. Furthermore, we define its (surface-based) counterpart for a triangulated boundary part of Ω by

$$\chi_s = V_s - E_s + F_s,$$

where V_s, E_s, and F_s are the vertices, edges, and faces located on the boundary part under consideration. For some sample volume and surface meshes, the values of the Euler characteristics are summarized in Table 1.

The incompressible Navier-Stokes equations describe the flow behavior of an incompressible and viscous fluid characterized by its velocity field $\mathbf{v} : \Omega \to \mathbb{R}^d$ and pressure variable $p : \Omega \to \mathbb{R}$ and read

$$\alpha\mathbf{v} + \rho(\mathbf{v}\cdot\nabla)\mathbf{v} - \mu\Delta\mathbf{v} + \nabla p = \rho\mathbf{g} \qquad \text{in } \Omega, \tag{1a}$$

$$\nabla\cdot\mathbf{v} = 0 \qquad \text{in } \Omega, \tag{1b}$$

$$\mathbf{v} = \mathbf{v}_\mathrm{D} \qquad \text{on } \Gamma_\mathrm{D}, \tag{1c}$$

$$-p\mathbf{n}_\Omega + \mu(\mathbf{n}_\Omega\cdot\nabla)\mathbf{v} = \rho\mathbf{h} \qquad \text{on } \Gamma_\mathrm{N}, \tag{1d}$$

where the Lipschitz boundary $\partial\Omega = \Gamma_\mathrm{D} \dot\cup \Gamma_\mathrm{N}$ of Ω is decomposed into its Dirichlet and Neumann boundary part. Furthermore, the Dirichlet boundary data is given by $\mathbf{v}_\mathrm{D} : \Gamma_\mathrm{D} \to \mathbb{R}^3$, while $\mathbf{g} : \Omega \to \mathbb{R}^3$ represents the body force density and $\mathbf{h} : \Gamma_\mathrm{N} \to \mathbb{R}^3$ is the force acting on the fluid in the outward normal direction $\mathbf{n}_\Omega : \partial\Omega \to \mathbb{R}^3$ [KH14, Chapter 8]. Finally, the dynamic viscosity μ and the density ρ are positive constants characterizing the Newtonian fluid, while the reactive contribution $\alpha\mathbf{v}$ for $\alpha > 0$ can be used to analyze time-dependent problems after discretization in time. For steady state problems, mainly considered in this work, we set $\alpha = 0$.

If $\Gamma_{\mathrm{N},1} \dot\cup \ldots \dot\cup \Gamma_{\mathrm{N},N_s}$, $N_s \in \mathbb{N}$, is a separated decomposition of Γ_N, then the Neumann boundary condition (1d) can be replaced by a flux boundary condition

$$\int_{\Gamma_{\mathrm{N},i}} \mathbf{n}_\Omega \cdot \mathbf{v} \,\mathrm{d}\mathbf{s} = f_{\mathrm{N},i} \tag{2}$$

for some net fluxes $f_{\mathrm{N},1}, \ldots, f_{\mathrm{N},N_s}$ through the surfaces $\Gamma_{\mathrm{N},1}, \ldots, \Gamma_{\mathrm{N},N_s}$, where

$$\sum_{i=1}^{N_s} f_{\mathrm{N},i} + \int_{\Gamma_\mathrm{D}} \mathbf{n}_\Omega \cdot \mathbf{v}_\mathrm{D} \,\mathrm{d}\mathbf{s} = \int_{\partial\Omega} \mathbf{n}_\Omega \cdot \mathbf{v} \,\mathrm{d}\mathbf{s} = \int_\Omega \nabla \cdot \mathbf{v} \,\mathrm{d}\mathbf{x} = 0 \tag{3}$$

must be satisfied by virtue of the continuity equation (1b). Note that a similar flow behavior can be achieved by enforcing a suitable auxiliary pressure condition for some values $p_1, \ldots, p_{N_s} \in \mathbb{R}$ (cf. [HRT96]), where the force $\mathbf{h}$ acting on the fluid is defined by

$$\mathbf{h} = \rho^{-1} \mathbf{n}_\Omega \sum_{i=1}^{N_s} p_i \chi_{\Gamma_{\mathrm{N},i}}$$

using the characteristic function $\chi_{\Gamma_{\mathrm{N},i}} : \partial\Omega \to \{0, 1\}$. This boundary condition can even be employed for discretely divergence-free finite elements, where the pressure variable is eliminated in an a priori manner. However, this approach does not yield further insight in the solution procedure and, hence, will be omitted in this paper for the sake of brevity.

Let us now introduce the finite element spaces of the Rannacher-Turek finite element pair. For this purpose, we first define the non-conforming rotated trilinear finite element space V_h in its non-parametric form [RT92]

$$\begin{aligned} V_h = \big\{ v \in L^2(\Omega) : v|_K \in \tilde{Q}_1(K) \,\forall K \in \mathcal{T}_h, \\ \gamma_{K_1 \cap K_2}(v|_{K_1}) = \gamma_{K_1 \cap K_2}(v|_{K_2}) \,\forall K_1, K_2 \in \mathcal{T}_h, K_1 \cap K_2 \in \mathcal{F}_h \big\}, \end{aligned}$$

where $\mathcal{F}_h$ is the set of faces of the triangulation $\mathcal{T}_h$, the interfacial mean value functional $\gamma_F(\cdot)$ reads

$$\gamma_F(v) = |F|^{-1} \int_F v \,\mathrm{d}\mathbf{s} \quad \forall F \in \mathcal{F}_h \tag{4}$$

and

$$\tilde{Q}_1(K) = \mathrm{span}\{1, x_1, x_2, x_3, x_1^2 - x_2^2, x_2^2 - x_3^2\}, \quad \mathbf{x} = (x_1, x_2, x_3)^\top \in K.$$

Obviously, the dimension of V_h coincides with the total number of faces F_v and a unique basis $\varphi_1, \ldots, \varphi_{F_v} \in V_h$ is characterized by

$$|F_1| \cdot \gamma_{F_1}(\varphi_{F_2}) = \int_{F_1} \varphi_{F_2} \, \mathrm{d}\mathbf{s} = \delta_{F_1,F_2} \quad \forall F_1, F_2 \in \mathcal{F}_h. \tag{5}$$

For the Rannacher-Turek finite element pair, each component of the velocity field is sought in V_h, while the pressure variable is approximated by piecewise constant functions, i.e.,

$$Q_h = \big\{ q \in L^2(\Omega) : v|_K \equiv c \, \forall K \in \mathcal{T}_h, c \in \mathbb{R} \big\}.$$

Therefore, the integral mean value of the divergence vanishes on each cell for the discrete velocity solution to the incompressible Navier-Stokes equations and the space of discretely divergence-free finite element functions reads

$$\mathbf{V}_h = \Big\{ \mathbf{v}_h \in (V_h)^3 : \int_K \nabla \cdot \mathbf{v}_h \, \mathrm{d}\mathbf{x} = 0 \, \forall K \in \mathcal{T}_h \Big\}.$$

This space can be decomposed into a subset of so called 'tangential' FE functions $\mathbf{V}_{\mathbf{t},h}$ and functions with non-trivial normal components on the faces, denoted by $\mathbf{V}_{\mathbf{n},h}$. These subspaces read

$$\begin{aligned} \mathbf{V}_{\mathbf{t},h} &= \big\{ \mathbf{v}_h \in \mathbf{V}_h : \gamma_F(\mathbf{v}_h \cdot \mathbf{n}_F) = 0 \, \forall F \in \mathcal{F}_h \big\}, \\ \mathbf{V}_{\mathbf{n},h} &= \big\{ \mathbf{v}_h \in \mathbf{V}_h : \gamma_F(\mathbf{v}_h \times \mathbf{n}_F) = \mathbf{0} \, \forall F \in \mathcal{F}_h \big\}, \end{aligned}$$

where $\mathbf{n}_F \in \mathbb{R}^3$ is a constant, but ambiguously defined unit normal vector of the face F under consideration. Then the finite element spaces have the following dimensions:

$$\dim(\mathbf{V}_h) = 3F_v - C_v, \quad \dim(\mathbf{V}_{\mathbf{t},h}) = 2F_v, \quad \dim(\mathbf{V}_{\mathbf{n},h}) = F_v - C_v =: S_v$$

Basis functions of $\mathbf{V}_{\mathbf{t},h}$ can be easily defined by introducing two unique tangential vectors $\mathbf{t}_1, \mathbf{t}_2$ per face (cf. [Hec81; Tho81]). However, the construction of a basis for the subspace $\mathbf{V}_{\mathbf{n},h}$ is a non-trivial task. One common approach is to first create a spanning set for $\mathbf{V}_{\mathbf{n},h}$ consisting of one function associated with each edge of the mesh. Afterwards $E_v - (F_v - C_v)$ functions associated with a spanning tree of the triangulation $\mathcal{T}_h$ are successively removed [Hec81]. Unfortunately, this graph-based approach to construct a basis only works for simply connected domains and, especially, fails for doughnut-shaped domains as we will see below. Therefore, another process for the construction of a basis has to be considered, which is discussed in what follows.

2.1 Construction of spanning set

For the sake of completeness, we first construct a basis of $\mathbf{V}_{\mathbf{t},h}$ using two unique tangential vectors for each face of the triangulation. The definition is only based on local mesh information and, hence, can be performed in an element-based fashion as usually preferred in the context of finite elements. For this purpose, let $\mathbf{x}_1, \ldots, \mathbf{x}_{V_v} \in \mathbb{R}^3$ be the vertices of the mesh ordered in an arbitrary, but unique manner. Then each face $F \in \mathcal{F}_h$ coincides with the

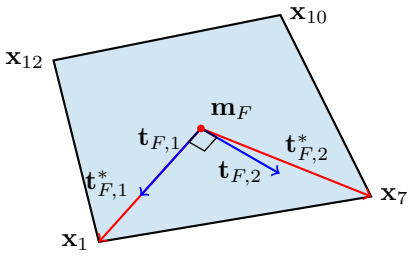

Figure 1: Construction of unique tangential vectors $\mathbf{t}_{F,1}$ and $\mathbf{t}_{F,2}$ for a face F with edges $\mathbf{x}_1$, $\mathbf{x}_7$, $\mathbf{x}_{10}$, and $\mathbf{x}_{12}$.

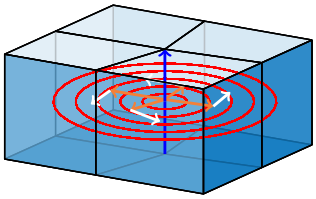

Figure 2: Streamlines of FE function $\boldsymbol{\psi}_E$ corresponding to edge plotted in blue. Associated normal vectors $\mathbf{n}_{E,F}$ are plotted in white.

convex hull of four vertices $\mathbf{x}_{i_1}, \dots, \mathbf{x}_{i_4}$ for $i_1, \dots, i_4 \in \{1, \dots, V_v\}$ and the midpoint $\mathbf{m}_F$ of F is defined by

$$\mathbf{m}_F = \tfrac{1}{4}(\mathbf{x}_{i_1} + \ldots + \mathbf{x}_{i_4}),$$

where $\mathbf{m}_F \in F$ holds true due to the fact that F is planar. Based on this definition, two orthonormal tangential vectors can be introduced by (cf. Fig. 1)

$$\begin{aligned}
\mathbf{t}^*_{F,1} &= \mathbf{x}_{i_j} - \mathbf{m}_F, \quad j = \operatorname*{arg\,min}_{\ell=1,\dots,4} i_\ell, \\
\mathbf{t}^*_{F,2} &= \mathbf{x}_k - \mathbf{m}_F, \quad k = \min\{i_{\mathrm{mod}(j,4)+1}, i_{\mathrm{mod}(j+2,4)+1}\}, \\
\mathbf{t}_{F,1} = \frac{\mathbf{t}^*_{F,1}}{\|\mathbf{t}^*_{F,1}\|_2}, &\quad \tilde{\mathbf{t}}^*_{F,2} = \mathbf{t}^*_{F,2} - (\mathbf{t}^*_{F,2} \cdot \mathbf{t}_{F,1})\mathbf{t}_{F,1}, \quad \mathbf{t}_{F,2} = \frac{\tilde{\mathbf{t}}^*_{F,2}}{\|\tilde{\mathbf{t}}^*_{F,2}\|_2}
\end{aligned}$$

and a basis $(\boldsymbol{\phi}_{F,1}, \boldsymbol{\phi}_{F,2})_{F \in \mathcal{F}_h}$ of $\mathbf{V}_{\mathbf{t},h}$ is uniquely defined by the condition

$$\int_F \mathbf{t}_{F_1,k} \cdot \boldsymbol{\phi}_{F_2,\ell} \, \mathrm{d}\mathbf{s} = \delta_{k,\ell}\delta_{F_1,F_2} \quad \forall F_1, F_2 \in \mathcal{F}_h,\ k, \ell \in \{1,2\}$$

leading to

$$\boldsymbol{\phi}_{F,\ell} = \mathbf{t}_{F,\ell}\varphi_F \quad \forall F \in \mathcal{F}_h,\ \ell \in \{1,2\}.$$

Indeed, these functions are discretely divergence-free due to

$$\int_K \nabla \cdot \boldsymbol{\phi}_{F,\ell} \, \mathrm{d}\mathbf{x} = \int_{\partial K} \mathbf{n}_K \cdot \boldsymbol{\phi}_{F,\ell} \, \mathrm{d}\mathbf{s} = \int_{\partial K} \underbrace{(\mathbf{n}_K \cdot \mathbf{t}_{F,\ell})}_{=0} \varphi_F \, \mathrm{d}\mathbf{s} = 0,$$

where $\mathbf{n}_K$ is the unit outward normal vector of cell $K \in \mathcal{T}_h$.

To construct a spanning set of $\mathbf{V}_{\mathbf{n},h}$, we first introduce 'normal' vectors $\mathbf{n}_{E,F}$ for all edges E and faces $F \in \mathcal{F}_h$

$$\mathbf{n}_{E,F} = \begin{cases} \frac{\mathbf{s}_E \times (\mathbf{m}_F - \mathbf{m}_E)}{\|\mathbf{s}_E \times (\mathbf{m}_F - \mathbf{m}_E)\|_2} & : E \subseteq F, \\ \mathbf{0} & : E \nsubseteq F, \end{cases}$$

where $\mathbf{s}_E = \mathbf{x}_k - \mathbf{m}_E$ is the vector pointing from the midpoint $\mathbf{m}_E = \frac{1}{2}(\mathbf{x}_{i_1} + \mathbf{x}_{i_2})$ of edge E with vertices $\mathbf{x}_{i_1}, \mathbf{x}_{i_2}$ to the vertex $\mathbf{x}_k$ with $k = \min\{i_1, i_2\}$. We then define $\boldsymbol{\psi}_E \in \mathbf{V}_{\mathbf{n},h}$ associated with an edge E by (cf. Fig. 2)

$$\boldsymbol{\psi}_E = \sum_{F \in \mathcal{F}_h} \mathbf{n}_{E,F} \varphi_F.$$

These functions have a local support $\operatorname{supp}(\boldsymbol{\psi}_E) = \bigcup_{K \in \mathcal{T}_h,\, E \subset K} K$ and satisfy

$$\int_F \mathbf{n}_F \cdot \boldsymbol{\psi}_E \,\mathrm{d}\mathbf{s} = \sum_{F' \in \mathcal{F}_h} (\mathbf{n}_F \cdot \mathbf{n}_{E,F'}) \underbrace{\int_F \varphi_{F'} \,\mathrm{d}\mathbf{s}}_{=\delta_{F,F'}} = \mathbf{n}_{E,F} \cdot \mathbf{n}_F \quad \forall F \in \mathcal{F}_h$$

This guarantees that $\boldsymbol{\psi}_E$ is discretely divergence-free because

$$\begin{aligned}\int_K \nabla \cdot \boldsymbol{\psi}_E \,\mathrm{d}\mathbf{x} &= \int_{\partial K} \mathbf{n}_K \cdot \boldsymbol{\psi}_E \,\mathrm{d}\mathbf{s} = \sum_{\text{face } F \subset \partial K} \int_F \mathbf{n}_K \cdot \boldsymbol{\psi}_E \,\mathrm{d}\mathbf{s} \\ &= \int_{F_1} \mathbf{n}_K \cdot \boldsymbol{\psi}_E \,\mathrm{d}\mathbf{s} + \int_{F_2} \mathbf{n}_K \cdot \boldsymbol{\psi}_E \,\mathrm{d}\mathbf{s} = (\mathbf{n}_{E,F_1} \cdot \mathbf{n}_K) + (\mathbf{n}_{E,F_2} \cdot \mathbf{n}_K) = 0\end{aligned}$$

for all elements $K \in \mathcal{T}_h$ with $E \subset K$, where the faces $F_1, F_2 \in \mathcal{F}_h$ are defined so that $F_1, F_2 \subset K$ and $F_1 \cap F_2 = E$.

For the sake of simplicity, we also refer to the FE function $\boldsymbol{\psi}_E$ using the notation $\boldsymbol{\psi}_i$, where i is the index of edge E. The functions $\boldsymbol{\psi}_1, \ldots, \boldsymbol{\psi}_{E_v}$ then span a subspace

$$\mathbf{V}^*_{\mathbf{n},h} = \operatorname{span}\{\boldsymbol{\psi}_1, \ldots, \boldsymbol{\psi}_{E_v}\} \subseteq \mathbf{V}_{\mathbf{n},h},$$

where equality is valid only for simply connected meshes. In case of arbitrary triangulations, this is not true because all functions in the subspace $\mathbf{V}^*_{\mathbf{n},h}$ have vanishing net fluxes on each closed boundary part of the domain. More precisely, the incompressibility condition

$$\oint_{\partial \varpi} \mathbf{n}_\varpi \cdot \mathbf{v}_h \,\mathrm{d}\mathbf{s} = 0 \quad \forall \varpi \subset \mathbb{R}^3,\, \partial\varpi \subseteq \bigcup_{F \in \mathcal{F}_h} F \tag{6}$$

is satisfied for all $\mathbf{v}_h \in \mathbf{V}^*_{\mathbf{n},h}$, where $\varpi \subset \mathbb{R}^3$ does not necessarily have to be a subset of Ω. For functions $\mathbf{v}_h \in \mathbf{V}_{\mathbf{n},h}$, property (6) is only true for $\varpi \subseteq \Omega$ and we have

$$\mathbf{V}^*_{\mathbf{n},h} = \big\{\mathbf{v}_h \in \mathbf{V}_{\mathbf{n},h} : \mathbf{v}_h \text{ satisfies condition (6)}\big\}.$$

Therefore, the dimension S^*_v of $\mathbf{V}^*_{\mathbf{n},h}$ is equal to S_v minus the number of holes in the domain (cf. Fig. 3 and Table 2). In the following section, we will construct a basis of the subspace of discretely divergence-free finite element functions $\mathbf{V}^*_h = \mathbf{V}_{\mathbf{t},h} \oplus \mathbf{V}^*_{\mathbf{n},h}$ by eliminating functions from the spanning set $\boldsymbol{\psi}_1, \ldots, \boldsymbol{\psi}_{E_v} \in \mathbf{V}^*_{\mathbf{n},h}$.

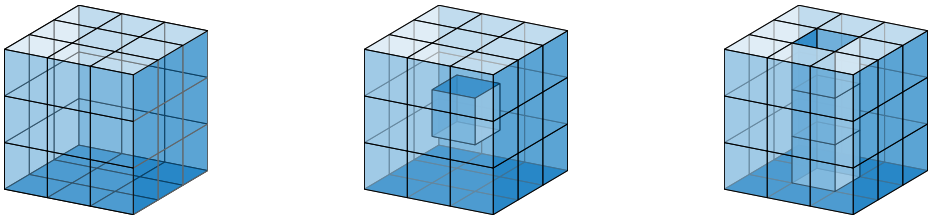

(a) Mesh I (uniform). (b) Mesh II (with hole). (c) Mesh III (doughnut-like).

Figure 3: Illustration of sample meshes with different topologies.

Table 2: Different quantities of sample meshes. Value of $H_v - 1$ describes number of separated holes and coincides with $S_v - S_v^* = \dim(\mathbf{V}_h) - \dim(\mathbf{V}_h^*)$.

	V_v	E_v	F_v	C_v	χ_v	H_v	S_v	S_v^*
Mesh I	64	144	108	27	1	1	81	81
Mesh II	64	144	108	26	2	2	82	81
Mesh III	64	144	104	24	0	1	80	80

2.2 Construction of basis

Some results for the construction of a basis can be found, e.g., in [GH83; For81; Gri81], while a very promising approach based on graph theory was published in [Hec81] for tetrahedral triangulations of simply connected domains. Therein, the author proved that functions $\boldsymbol{\psi}_E$ associated with edges E of a spanning tree have to be removed to create a basis. The spanning tree of a connected graph has $V_v - 1$ edges and is defined as the minimal graph connecting all vertices of a mesh without closed paths. Unfortunately, this idea only works for simply connected domains and, especially, not for doughnut-shaped domains. In the latter case, the functions after the elimination process are still linearly dependent and, hence, not a basis. This can be easily verified by dimension counting arguments: We first notice that $\mathbf{V}_{\mathbf{n},h}^* = \mathbf{V}_{\mathbf{n},h}$ is valid because the entire boundary is connected. Therefore, in total $E_v - S_v$ functions have to be removed from the spanning set, where $S_v = F_v - C_v = \dim(\mathbf{V}_{\mathbf{n},h})$. On the other hand, the number of edges of the spanning tree coincides with

$$V_v - 1 = V_v - 1 - \chi_v = E_v - F_v + C_v - 1 = E_v - S_v - 1$$

due to the fact that the Euler characteristic $\chi_v = V_v - E_v + F_v - C_v$ is equal to 0 for doughnut-shaped domains. Therefore, another basis function associated with an additional edge $\hat{E}$ has to be removed. Adding this extra edge to the spanning tree must result in a closed path around the 'hole' of the domain. However, finding $\hat{E}$ is a non-trivial task and requires knowledge about the minimal graph *and* the topology of the mesh.

The algorithm proposed in [Hec81] constructing the spanning tree is summarized in Algorithm 1. It just expoits the connectivity graph of the triangulation without any knowledge about the cells and faces of the mesh. While the algorithm also seems to work perfectly for meshes with holes, the procedure fails for doughnut-shaped domains. Especially, the different

Algorithm 1 Construction of basis $(\boldsymbol{\psi}_E)_{E\notin\mathcal{H}}$ to $\mathbf{V}^*_{\mathbf{n},h}$ for simply connected domain as described in [Hec81; Tho81].

Ensure: Output $\mathcal{H}$
  Initialize $\mathcal{H} \leftarrow \emptyset$
  for $i \leftarrow 1$ to V_v **do**
    $M(i) \leftarrow i$
  end for
  for edge $E \subset \partial\Omega$ **do**
    Call **SP**(E)
  end for
  for all other edges E **do**
    Call **SP**(E)
  end for

Procedure: SP(E)
$i, j \leftarrow$ vertices of edge E
if $M(i) \neq M(j)$ **then**
  $\mathcal{H} \leftarrow \mathcal{H} \cup \{E\}$
  $m_j \leftarrow M(j)$
  for $k \leftarrow 1$ to V_v **do**
    if $M(k) = m_j$ **then**
      $M(k) \leftarrow M(i)$
    end if
  end for
end if

shapes of the meshes illustrated in Fig. 3 are not 'recognized' and lead to the same spanning tree. Based on this graph, it is hardly possible to find an additional edge $\hat{E}$ for Mesh III, which results in a basis for $\mathbf{V}^*_{\mathbf{n},h}$. Therefore, we discuss another approach to define a basis, which is motivated by a constructional way to uniquely represent some function $\mathbf{v}_h \in \mathbf{V}^*_{\mathbf{n},h}$ in terms of the discretely divergence-free FE functions $\boldsymbol{\psi}_1, \ldots, \boldsymbol{\psi}_{E_v}$

$$\mathbf{v}_h = \sum_{i=1}^{E_v} v_i \boldsymbol{\psi}_i = \sum_{\text{edge } E} v_E \boldsymbol{\psi}_E,$$

where $v_1, \ldots, v_{E_v} \in \mathbb{R}$ or $(v_E)_{\text{edge } E}$ are the degrees of freedom to be defined. For this purpose, we note that $\mathbf{v}_h \in \mathbf{V}^*_{\mathbf{n},h}$ is uniquely determined by the normal flux through all faces $F \in \mathcal{F}_h$

$$f_F = \int_F \mathbf{n}_F \cdot \mathbf{v}_h \, \mathrm{d}\mathbf{s} \quad \forall F \in \mathcal{F}_h.$$

On the other hand, the normal flux through a face $F \in \mathcal{F}_h$ satisfies

$$\int_F \mathbf{n}_F \cdot \mathbf{v}_h \, \mathrm{d}\mathbf{s} = \sum_{\text{edge } E} v_E \int_F \mathbf{n}_F \cdot \boldsymbol{\psi}_E \, \mathrm{d}\mathbf{s} = \sum_{\text{edge } E \subset \partial F} v_E \underbrace{(\mathbf{n}_{E,F} \cdot \mathbf{n}_F)}_{=\pm 1} \quad \forall F \in \mathcal{F}_h \tag{7}$$

for any function $\mathbf{v}_h \in \mathcal{V}^*_{\mathbf{n},h}$ represented by the set of discretely divergence-free functions $\boldsymbol{\psi}_1, \ldots, \boldsymbol{\psi}_{E_v}$ and, hence, coincides with a (weighted) sum over the adjoined four edges (cf. [Gri81]). Therefore, the condition

$$f_F = \sum_{\text{edge } E \subset \partial F} v_E (\mathbf{n}_{E,F} \cdot \mathbf{n}_F) \tag{8}$$

must be satisfied for all faces $F \in \mathcal{F}_h$ in order to represent a function $\mathbf{v}_h \in \mathbf{V}^*_{\mathbf{n},h}$ in terms of the functions $\boldsymbol{\psi}_1, \ldots, \boldsymbol{\psi}_{E_v}$. According to (6), this identity is automatically true for a face $F \in \mathcal{F}_h$ if it is valid for faces $F_1, \ldots, F_k \in \mathcal{F}_h$, $k \in \mathbb{N}$, such that $F \cup F_1 \cup \ldots \cup F_k$ is a closed surface. Inspired by these ideas, a basis of $\mathbf{V}^*_{\mathbf{n},h}$ can be characterized as follows:

Let $F_1, \dots, F_{S_v^*} \in \mathcal{F}_h$ be a list of faces so that $\bigcup_{i=1}^{S_v^*} F_i$ does not contain a closed surface and let the edges $E_1, \dots, E_{E_v}$ be ordered so that

$$E_i \subset \partial F_i \subset \Big(\bigcup_{j=1}^{i} E_j\Big) \cup \Big(\bigcup_{j=S_v^*+1}^{E_v} E_j\Big) \quad \forall i \in \{1, \dots, S_v^*\}. \tag{9}$$

Then the functions $\boldsymbol{\psi}_1, \dots, \boldsymbol{\psi}_{S_v^*}$ associated with the edges $E_1, \dots E_{S_v^*}$ form a basis of $\mathbf{V}^*_{\mathbf{n},h}$.

The maximum number of faces S_v^* not creating a closed surface can be easily verified by considering the complement of the spanning tree for a graph, whose nodes and edges are given by the cells and faces of the mesh, respectively. Furthermore, additional nodes have to be included for each separated void of the domain (holes and surrounded area). Then the spanning tree has $G_v - 1$ edges, where G_v is the number of nodes, i.e., number of cells C_v plus number of connected components of Ω^c, denoted by H_v. Thus, the total number of faces S_v^* not creating a closed surface is given by

$$S_v^* = F_v - (G_v - 1) = F_v - C_v - H_v + 1 = S_v - H_v + 1.$$

If the list of faces $F_1, \dots, F_{S_v^*}$ and edges $E_1, \dots, E_{E_v}$ satisfies the above statement, then we can iterate over the faces and define the degrees of freedom $v_1, \dots, v_{S_v^*}$ one after the other by (8), while $v_{S_v^*+1}, \dots, v_{E_v}$ can be chosen arbitrarily. Indeed, the definitions of

$$v_i = (\mathbf{n}_{F_i} \cdot \mathbf{n}_{i,F_i})^{-1} \Big(f_{F_i} - \sum_{e=1}^{i-1} (\mathbf{n}_{F_i} \cdot \mathbf{n}_{e,F_i}) v_e \Big) \quad \forall i \in \{1, \dots, S_v^*\}$$

and $v_{S_v^*+1} = \dots = v_{E_v} = 0$ guarantee that

$$\begin{aligned} \int_{F_i} \mathbf{n}_{F_i} \cdot \mathbf{v}_h \, \mathrm{d}\mathbf{s} &= \sum_{e=1}^{S_v^*} v_e \int_{F_i} \mathbf{n}_{F_i} \cdot \boldsymbol{\psi}_e \, \mathrm{d}\mathbf{s} \\ &= \sum_{e=1}^{S_v^*} v_e (\mathbf{n}_{F_i} \cdot \mathbf{n}_{e,F_i}) = \sum_{e=1}^{i} v_e (\mathbf{n}_{F_i} \cdot \mathbf{n}_{e,F_i}) = f_{F_i} \quad \forall i \in \{1, \dots, S_v^*\} \end{aligned}$$

due to the fact that all faces are planar. Furthermore,

$$\int_{F_i} \mathbf{n}_{F_i} \cdot \mathbf{v}_h \, \mathrm{d}\mathbf{s} = f_{F_i} \quad \forall i \in \{S_v^* + 1, \dots, F_v\}$$

is trivially satisfied due to the fact that $\big(\bigcup_{j=1}^{S_v^*} F_j\big) \cup F_i$ contains a closed surface for all $i = S_v^* + 1, \dots, F_v$.

2.3 Boundary conditions

After the definition of a basis for the spaces of discretely divergence-free finite element functions $\mathbf{V}_{\mathbf{t},h}$ and $\mathbf{V}^*_{\mathbf{n},h}$, we now discuss how Dirichlet boundary conditions can be prescribed

and why geometries introducing bifurcations require a special treatment. The enforcement of boundary conditions for the tangential subspace $\mathbf{V}_{\mathbf{t},h}$ can be performed in a straightforward manner. Therefore, we solely focus on the normal contribution of the boundary data, which is associated with the subspace $\mathbf{V}^*_{\mathbf{n},h}$. For a simply connected domain with Dirichlet boundary conditions prescribed on the entire boundary, Hecht [Hec81] mentioned that the number of basis functions corresponding to edges located on the boundary part of the domain should be minimized. This design criterion is already taken into account in the construction process of a spanning tree using Algorithm 1 by first considering the edges located on the boundary of Ω. It guarantees that the total number of degrees of freedom associated with the Dirichlet boundary part coincides with the number of prescribed normal components

$$\int_F \mathbf{n}_F \cdot \mathbf{v}_\mathrm{D} \,\mathrm{d}\mathbf{s} = \int_F \mathbf{n}_F \cdot \mathbf{v}_h \,\mathrm{d}\mathbf{s} \quad \forall F \in \mathcal{F}_h,\, F \cap \Gamma_\mathrm{D} \neq \emptyset.$$

This can be easily verified using the Euler characteristic for a surface of a closed convex polyhedron

$$\chi_s = V_s - E_s + F_s = 2,$$

where V_s, E_s, and F_s denote the number of vertices, edges, and faces located on the Dirichlet boundary part. Then $E_s - (V_s - 1) = F_s - 1$ basis functions are associated with edges located on the boundary $\partial\Omega$ due to the fact that the spanning tree of the boundary part has $V_s - 1$ edges. This is indeed the number of independent normal contributions, which have to be prescribed, because the boundary part Γ_D consists of F_s faces and one normal contribution is automatically determined by the others due to the incompressibility condition (6) for $\varpi = \Omega$.

This concept for prescribing Dirichlet boundary conditions also holds true for simply connected domains with one connected Neumann boundary part. In this case, the Euler characteristic of Γ_D reads

$$\chi_s = V_s - E_s + F_s = 1$$

and $E_s - (V_s - 1) = F_s$ degrees of freedom can be uniquely determined by F_s conditions for the flow through the faces on the Dirichlet boundary part.

In the numerical examples, we will also consider the flow through a "y-pipe" featuring two separate Neumann boundary parts $\Gamma_{\mathrm{N},1}$ and $\Gamma_{\mathrm{N},2}$. In this case, the strategy mentioned above fails without further modifications although the mesh itself is simply connected. This is due to the fact that the Euler characteristic of the Dirichlet boundary part $\Gamma_\mathrm{D} = \partial\Omega \setminus (\Gamma_{\mathrm{N},1} \cup \Gamma_{\mathrm{N},2})$ satisfies

$$\chi_s = V_s - E_s + F_s = 0$$

leading to (at least) $E_s - (V_s - 1) = F_s + 1$ basis functions associated with the Dirichlet boundary part, while only F_s normal contributions have to be prescribed. This apparent discrepancy stems from the fact that the net fluxes through $\Gamma_{\mathrm{N},1}$ and $\Gamma_{\mathrm{N},2}$ are solely determined by edges located on $\Gamma_{\mathrm{N},1} \cap \Gamma_\mathrm{D}$ and $\Gamma_{\mathrm{N},2} \cap \Gamma_\mathrm{D}$, respectively. Therefore, setting all solution coefficients associated with Γ_D also prescribes the fluxes through the Neumann boundary parts. To enable the independent enforcement of flux or Neumann boundary conditions without modifying the normal contributions on Γ_D, we introduce a so called 'global' function $\boldsymbol{\psi}_{\mathrm{N},1} \in \mathbf{V}^*_{\mathbf{n},h}$. For this purpose, let $F_1, \ldots, F_{F_s}$ be the faces located on the

Dirichlet boundary part of the domain and $\boldsymbol{\psi}_1, \ldots, \boldsymbol{\psi}_{F_s+1}$ be the basis functions associated with edges located on Γ_D. Then $\boldsymbol{\psi}_{\mathrm{N},1} = \sum_{i=1}^{F_s+1} v_{i,1} \boldsymbol{\psi}_i$ is defined by

$$\int_{F_i} \mathbf{n}_\Omega \cdot \boldsymbol{\psi}_{\mathrm{N},1} \,\mathrm{d}\mathbf{s} = 0 \quad \forall i \in \{1, \ldots, F_s\}, \qquad \int_{\Gamma_{\mathrm{N},1}} \mathbf{n}_\Omega \cdot \boldsymbol{\psi}_{\mathrm{N},1} \,\mathrm{d}\mathbf{s} = 1. \tag{10}$$

We now replace $\boldsymbol{\psi}_{i_0}$ for some $i_0 \in \{1, \ldots, F_s + 1\}$ satisfying $v_{i_0,1} \neq 0$ with $\boldsymbol{\psi}_{\mathrm{N},1}$ and achieve another basis of $\mathbf{V}^*_{\mathbf{n},h}$. Thus, flux boundary conditions can be prescribed by setting the solution coefficient $v_{\mathrm{N},1}$ associated with $\boldsymbol{\psi}_{\mathrm{N},1}$. This process is particularly simple, if $\boldsymbol{\psi}_{i_0}$ is the only basis function associated with an edge E_{i_0} located on $\Gamma_{\mathrm{N},1} \cap \Gamma_\mathrm{D}$. Then the flux through $\Gamma_{\mathrm{N},1}$ collapses to

$$\int_{\Gamma_{\mathrm{N},1}} \mathbf{n}_\Omega \cdot \mathbf{v}_h \,\mathrm{d}\mathbf{s} = v_{\mathrm{N},1} \underbrace{\int_{\Gamma_{\mathrm{N},1}} \mathbf{n}_\Omega \cdot \boldsymbol{\psi}_{\mathrm{N},1} \,\mathrm{d}\mathbf{s}}_{=1} + \sum_{i=1, i\neq i_0}^{S_v^*} v_i \underbrace{\int_{\Gamma_{\mathrm{N},1}} \mathbf{n}_\Omega \cdot \boldsymbol{\psi}_i \,\mathrm{d}\mathbf{s}}_{=0} = v_{\mathrm{N},1} \tag{11}$$

and the boundary condition (2) can readily be enforced by setting $v_{\mathrm{N},1} = f_{\mathrm{N},1}$.

On the other hand, the 'global' basis function $\boldsymbol{\psi}_{\mathrm{N},1}$ is treated as an 'inner' basis function when the Neumann boundary condition (1d) is prescribed. This is due to the fact that $\boldsymbol{\psi}_{\mathrm{N},1}$ does not contribute to the normal contributions on the Dirichlet boundary part. Note that in iterative solution procedures there is no need to assemble the discrete problem using this 'global' function. Instead, a suitable "projection method" can be employed to recover the validity of the correct boundary conditions in each iteration [CSS86].

The idea described above can be easily extended to problems, where Γ_N is a decomposition of $N_s > 2$ separated boundary parts $\Gamma_{\mathrm{N},1}, \ldots, \Gamma_{\mathrm{N},N_s}$. In this case, $N_s - 1$ 'global' functions $\boldsymbol{\psi}_{\mathrm{N},1}, \ldots, \boldsymbol{\psi}_{\mathrm{N},N_s-1}$ have to be introduced due to the fact that the net flux through Γ_{N,N_s} is automatically fulfilled by condition (3). Even doughnut-shaped domains can be considered in this way by introducing two auxiliary Neumann boundary parts, which split Ω into two simply connected subdomains. Finally, boundary conditions on several separated boundary parts can obviously be enforced by treating each of them in a segregated manner.

As mentioned above, the choice of the basis functions plays a crucial rule when it comes to the treatment of boundary conditions. Even in case of a simply connected domain with Dirichlet boundary conditions everywhere, it is important to minimize the number of basis functions associated with edges located on the boundary of the domain [Hec81]. Consequently, the construction of a set of basis functions must carefully take into account the boundary conditions to be prescribed. One promising strategy for more general meshes is to adapt Algorithm 1 by first treating the edges located on $\Gamma_\mathrm{D} \cap \Gamma_\mathrm{N}$. This guarantees that flux boundary conditions can be easily prescribed using (11). Furthermore, the construction of the list of faces as mentioned in (9) should be directly included in the algorithm. Here, closed surfaces can be avoided by using the spanning tree of a graph, whose nodes and edges are given by the cells and faces of the mesh, respectively. By considering the edges and faces in an element-wise manner, the graph-based approach exploited in Algorithm 1 remains valid as long as the union of the cells treated so far is simply connected. Finally, the set of functions only has to be reduced if Ω is not simply connected.

3 Multigrid solution technique

In this section, we introduce a geometric multigrid solution technique for the incompressible Navier-Stokes equations discretized by discretely divergence-free FE functions. The algorithm presented below mainly exploits the spanning set as introduced in Section 2.1, although more efficient approaches might be possible if the total number of degrees of freedom is reduced. A set of basis functions is only employed on the coarsest grid of the mesh hierarchy, while this information is extrapolated to finer grids for the enforcement of boundary conditions. Another nontrivial component of the multigrid solver is the prolongation operator, which should preserve at least globally linear, divergence-free functions to ensure a rapid convergence while avoiding excessive computational costs.

3.1 Intergrid transfer operator

The intergrid transfer operators play a crucial role in the design of efficient multigrid solution techniques. While the restriction operator is readily defined as the adjunct prolongation operator, the latter one should be as accurate as possible and preserve at least globally linear functions. For discretely divergence-free functions, the construction of an operator satisfying the above mentioned design criterion is quite intricate due to the fact that the trilinear finite element space under investigation is non-conforming, i.e., $V_h \nsubseteq V_{2h}$. Furthermore, a discretely divergence-free FE function defined on a coarse grid triangulation $\mathcal{T}_{2h}$ is generally not discretely divergence-free with respect to $\mathcal{T}_h$. In this paper, we follow an idea proposed in [Tur94a; Tur94b] for the two-dimensional Rannacher-Turek FE space, which highly exploits a prolongation operator for the FE function in its mixed form. In this process, the degrees of freedom of the fine grid velocity field are computed using the interfacial mean value functional γ_F for each cell and a subsequent averaging process if cells share a common interface.

Inspired by [Tur94a; Tur94b], the prolongation process to project a discretely divergence-free FE function $\mathbf{v}_{2h} \in \mathbf{V}_{2h}^*$ into $\mathbf{V}_h^*$ then reads as follows:

1. Compute projection $\tilde{\mathbf{v}}_h \in (V_h)^3$ of coarse grid function $\mathbf{v}_{2h} \in \mathbf{V}_{2h}^*$.
2. Determine tangential components $(v_h^{\mathbf{t}_1}, v_h^{\mathbf{t}_2})$ of $\tilde{\mathbf{v}}_h$ for all faces of fine grid.
3. Calculate normal coefficients $v_h^{\mathbf{n}}$ using normal fluxes of $\tilde{\mathbf{v}}_h$ through faces of fine grid.

We now focus on the last step of the prolongation procedure, which is most involved due to the fact that the interpolated fine grid solution is generally not discretely divergence-free with respect to $\mathcal{T}_h$. For this purpose, we subdivide the normal coefficients $v_h^{\mathbf{n}}$ into three categories: The ones associated with edges located on macro edges, on macro faces, and in the interior of the macro elements, as illustrated in Fig. 4a. Then the coefficients are computed one after the other as follows:

a) The degrees of freedom associated with edges located on an edge $\bar{E}$ of the coarse grid $\mathcal{T}_{2h}$ are set to (cf. Fig. 4b)

$$v_{h,E}^{\mathbf{n}} = \tfrac{1}{2}\,\mathrm{sign}(\mathbf{s}_E \cdot \mathbf{s}_{\bar{E}}) v_{2h,\bar{E}}^{\mathbf{n}} \quad \forall \text{edge } E \text{ of } \mathcal{T}_h,\ E \subset \bar{E}.$$

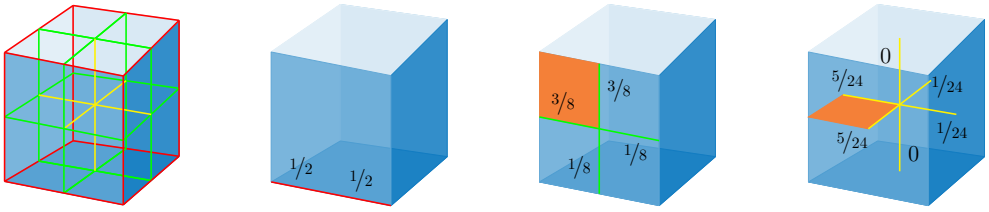

(a) Classification of fine-grid edges. (b) Step 1: coarse grid edges. (c) Step 2: coarse grid faces. (d) Step 3: interior edges.

Figure 4: Classification of different edges after uniform refinement and illustration of prolongation process including absolute weights of edge/face contributions to coefficient vector.

b) For each face of the coarse grid $\bar{F} \in \mathcal{F}_{2h}$, we create the linear system (cf. Fig. 4c)

$$\sum_{\text{edge } E \subset \partial F \setminus \partial \bar{F}} v_E(\mathbf{n}_{E,F} \cdot \mathbf{n}_F) = \int_F \mathbf{n}_F \cdot \tilde{\mathbf{v}}_h \, \mathrm{d}\mathbf{s} - \sum_{\text{edge } E \subset \partial \bar{F}} v_E(\mathbf{n}_{E,F} \cdot \mathbf{n}_F) \qquad \forall F \in \mathcal{F}_h,\ F \subset \bar{F}.$$

Then the coefficients associated with edges located on the face $\bar{F}$ are computed by solving the problem using the Moore-Penrose pseudoinverse.

c) For the degrees of freedom corresponding to edges located in the interior of a macro cell $\bar{K} \in \mathcal{T}_{2h}$, the associated linear system reads (cf. Fig. 4d)

$$\sum_{\text{edge } E \subset \partial F \setminus \partial \bar{K}} v_E(\mathbf{n}_{E,F} \cdot \mathbf{n}_F) = \int_F \mathbf{n}_F \cdot \tilde{\mathbf{v}}_h \, \mathrm{d}\mathbf{s} - \sum_{\text{edge } E \subset \partial \bar{K}} v_E(\mathbf{n}_{E,F} \cdot \mathbf{n}_F) \qquad \forall F \in \mathcal{F}_h,\ F \subset \bar{K} \setminus \partial \bar{K},$$

whose solution is approximated by exploiting again the Moore-Penrose pseudoinverse.

Step a) guarantees that the normal flux through the faces of the coarse grid is preserved

$$\int_{\bar{F}} \mathbf{n}_F \cdot \mathbf{v}_h \, \mathrm{d}\mathbf{s} = \int_{\bar{F}} \mathbf{n}_F \cdot \tilde{\mathbf{v}}_h \, \mathrm{d}\mathbf{s} = \int_{\bar{F}} \mathbf{n}_F \cdot \mathbf{v}_{2h} \, \mathrm{d}\mathbf{s} \quad \forall \bar{F} \in \mathcal{F}_{2h}.$$

This property is actually satisfied for all faces $F \cap \bar{F}$ with $F \in \mathcal{F}_h$, $\bar{F} \in \mathcal{F}_{2h}$ by virtue of Step b). Note that the solution to this problem exists, but is not unique. Therefore, you can either arbitrarily specify one degree of freedom per face $\bar{F}$ or use the Moore-Penrose pseudoinverse to determine a unique solution. The remaining six coefficients associated with edges in the interior of each macro cell $\bar{K} \in \mathcal{T}_{2h}$ are chosen so that the normal flux through the inner 12 faces is preserved in a least squares sense by Step c). Note that this problem is overdetermined and generally no solution exists due to the fact that $\tilde{\mathbf{v}}_h$ does not have to be discretely divergence-free with respect to $\mathcal{T}_h$. However, if $\tilde{\mathbf{v}}_h \in \mathbf{V}_h^*$, then the above mentioned procedure guarantees that $\mathbf{v}_h = \tilde{\mathbf{v}}_h$ and, especially, we have $\mathbf{v}_h = \mathbf{v}_{2h}$ for all $\mathbf{v}_{2h} \in \mathbf{V}_{2h}^* \cap \mathbf{V}_h^*$.

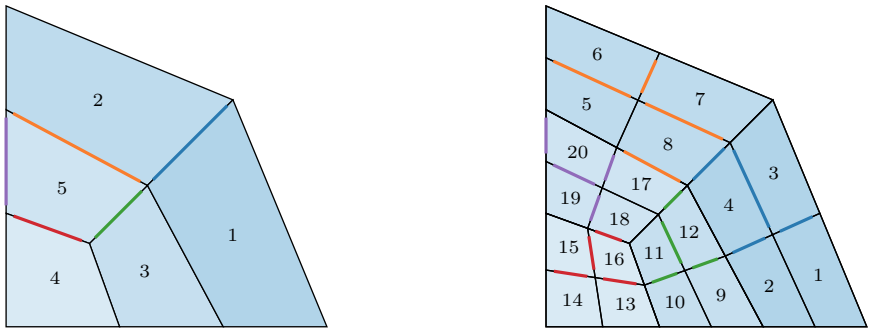

(a) Coarse grid. (b) Fine grid.

Figure 5: Finding basis of normal contribution associated with Dirichlet boundary part after one uniform grid refinement step. Edges associated with basis functions are highlighted in color.

3.2 Boundary conditions

In Section 2.3, a procedure to enforce different kinds of boundary conditions was presented, which highly exploits the explicit knowledge about a basis for the space of discretely divergence-free FE functions. Unfortunately, the construction of such a set of basis functions is a complex task and should be avoided on finer mesh levels. Therefore, we now outline a strategy to prescribe boundary conditions, which only exploits the basis on the coarsest level of a mesh hierarchy and extrapolates this information to finer grids. This procedure provides a set of linear independent functions on the Dirichlet boundary part of the domain so that the normal coefficients can be determined uniquely. For the sake of simplicity, we describe the idea just for two consecutive meshes, that is, $\mathcal{T}_h$ is obtained after one uniform refinement of the coarse grid $\mathcal{T}_{2h}$. However, it can easily be extended to more than two mesh levels.

First of all, we define a set of linear independent functions, which are associated with the boundary part of the domain and provide a unique way to determine the corresponding coefficients using the Dirichlet boundary data. For this purpose, we first assume that each face $\bar{F} \in \mathcal{F}_{2h}$ located on the Dirichlet boundary part of the domain, i.e., $\bar{F} \subseteq \Gamma_{\mathrm{D}}$, is associated with an edge $\bar{E} \subset \partial\bar{F}$ by (9). In the refinement process, the face $\bar{F}$ and edge $\bar{E}$ are decomposed into four faces $F_1, \dots, F_4$ and two edges E_0 and E_4, respectively. Without loss of generality, let us assume that $E_4 \subset \partial F_4$. Then there exist edges E_1, E_2, and E_3 so that the coefficients associated with $E_1, \dots, E_4$ can uniquely be determined using the normal fluxes through the faces $F_1, \dots, F_4$ and the associated basis functions are linearly independent (cf. Fig. 5). In this way, all edges associated with faces $F \in \mathcal{F}_h$ for $F \subseteq \Gamma_{\mathrm{D}}$ can be treated one after the other and only coefficients associated with 'global' basis functions remain undefined.

The concept of 'global' functions is required to either prescribe Neumann and flux boundary conditions or is used to determine the correct flow through doughnut-shaped domains (cf. Section 4.3). Such a function $\bar{\boldsymbol{\psi}}_{\mathrm{N},i} \in \mathbf{V}^*_{\mathbf{n},2h}$ is defined by property (10) and, roughly speaking, controls the flux through an interface $\Gamma_{\mathrm{N},i}$ without influencing the Dirichlet

boundary data of the FE solution. This property is preserved only approximately when $\bar{\boldsymbol{\psi}}_{\mathrm{N},i}$ is projected to $\mathcal{T}_h$ using the prolongation procedure described in Section 3.1. To exactly guarantee vanishing normal fluxes through the faces $F \in \mathcal{F}_h$ of the fine grid, Step b) of the prolongation process has to be adapted accordingly. Finally, the support of the resulting function $\boldsymbol{\psi}_{\mathrm{N},i}$ can be minimized by setting degrees of freedom not associated with edges located on boundary to zero. In an iterative solution process, the solution coefficients associated with these functions are then either known due to flux boundary conditions or by a suitable initial guess. In the latter case, the net flux through $\Gamma_{\mathrm{N},i}$ is finally corrected in each iteration using an adequate projection technique.

4 Numerical examples

In this section, we evaluate the concept of discretely divergence-free finite elements in three dimensions and, especially, the behavior of the multigrid solution technique introduced above. For this purpose, we investigate several test cases for different computational domains (cf. Fig. 6). We restrict ourselves to linear problems and either consider the incompressible Stokes or Oseen equations, where the velocity field of the convective term coincides with the solution to the incompressible Navier-Stokes equations. If not mentioned otherwise, we are focusing on the steady-state versions of the governing equations by neglecting the reactive term, that is, $\alpha = 0$. Note that the accuracy of the solution is solely determined by the Rannacher-Turek FE pair and is not affected by the solution technique utilizing discretely divergence-free finite elements. Therefore, results illustrating the accuracy of the discretization are omitted in this work and we refer to [ST94; Tur99] for detailed numerical studies.

The multigrid solver is always executed using an F-cycle, where the coarsest level corresponds to mesh level $\mathrm{lvl} = 0$ and the initial guess is given by a random vector with values uniformly distributed in $[0, 1]$. For pre- and post-smoothing, we either perform ν (damped) Richardson iterations (denoted by 'Richardson smoother') or a GMRES method using a fixed number of ν iterations (denoted by 'GMRES smoother'). In both cases, we employ the Jacobi or Gauß-Seidel preconditioner with a relaxation parameter of $\omega = 0.5$ or $\omega = 1$, respectively. According to the use of non-conforming finite elements, a step length control is optionally applied in the coarse grid correction [PB87; BV90; Tur94a], where the solution update is scaled by $\alpha_t \in [0.001, 2]$ to minimize the energy of the solution (denoted by 'adaptive coarse grid correction'). Otherwise, the coarse grid solution is added to the iterate without any scaling (denoted by 'full coarse grid correction').

To investigate the convergence behavior of the multigrid method, we perform a maximum number of 50 iterations and estimate the (asymptotic) rate of convergence by analyzing the last five iterates before the norm of the residual r_i reaches $100 \cdot r_{\min}$, where $r_{\min}$ is the minimal norm of the residual attained in the solution process, i.e., $r_{\min} = \min_{i \in \{1,\dots,50\}} r_i$. More precisely, we define the experimental rate of convergence ϱ by

$$\varrho = \sqrt[\delta t]{\frac{r_{t_0}}{r_{t_0-\delta t}}}, \quad t_0 = \max\big\{t \in \{2,\dots,T\} : r_t \geq 100 \cdot r_T\big\}, \quad \delta t = \min(4, t_0 - 2).$$

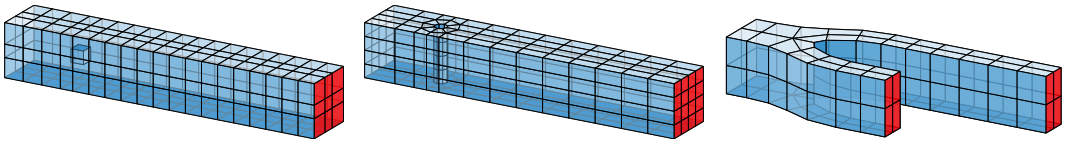

(a) Flow around cube. (b) Flow around cylinder. (c) Flow through y-pipe.

Figure 6: Coarse grid for different test cases. Neumann boundary parts are marked in red.

Table 3: Lid driven cavity: Comparison of total number of degrees of freedom and nonzero matrix entries for discretely divergence-free finite elements and mixed formulation.

	mesh information				DDFFE			mixed form.	
	V_v	E_v	F_v	C_v	$\dim(\mathbf{V}_h^*)$	#dofs	nnz	#dofs	nnz
$\text{lvl}=0$	27	54	36	8	100	126	3.97e3	116	2.77e3
$\text{lvl}=1$	125	300	240	64	656	780	3.05e4	784	2.17e4
$\text{lvl}=2$	729	1944	1728	512	4672	5400	2.38e5	5696	1.72e5
$\text{lvl}=3$	4913	13 872	13 056	4096	35 072	39 984	1.88e6	43 264	1.37e6
asympt.		$3V_v$	$3V_v$	V_v	$8V_v$	$9V_v$	$471V_v$	$10V_v$	$333V_v$

4.1 Lid driven cavity

We start our numerical investigations by considering the well-known *watertight lid driven cavity* test case, where the domain $\Omega = (0,1)^3$ is uniformly decomposed into $8^{\text{lvl}+1}$ cells on mesh level $\text{lvl} \in \{0,1,2,\dots\}$. Each mesh has asymptotically $3V_v$ edges, $3V_v$ faces, and V_v cells resulting in $6V_v$ and $3V_v$ functions spanning $\mathbf{V}_{\mathbf{t},h}$ and $\mathbf{V}_{\mathbf{n},h}^*$, respectively. The corresponding (singular) system matrix using discretely divergence-free finite elements consists of $471V_v$ nonzero entries, which is about 50% larger than in case of a mixed formulation assuming that all components of the velocity field interact with each other (cf. Table 3).

For the problem under investigation, Dirichlet boundary data

$$\mathbf{v}_{\mathrm{D}}(\mathbf{x}) = \begin{cases} (1,0,0)^\top & : x_2 = 1,\ x_1, x_3 \in (0,1), \\ (0,0,0)^\top & : \text{otherwise} \end{cases}$$

are strongly enforced on the entire boundary $\Gamma_{\mathrm{D}} = \partial\Omega$. Furthermore, the viscosity parameter μ is set to 0.01 while the convective term of the momentum equation is neglected resulting in the incompressible Stokes equations mimicking a Reynolds number of $\mathrm{Re} = 0$. For this setup, the convergence behavior of a basic multigrid algorithm employing a Richardson smoother with Jacobi preconditioning and no adaptive coarse grid correction is illustrated in Fig. 7. Even for this simple multigrid configuration, the convergence behavior does not depend on the level of refinement and the experimental rate of convergence is close to $\varrho = 0.3$ before the residual stagnates. Note that the absolute value of the residual grows with respect to the level of refinement according to the scaling of the basis functions defined in (5).

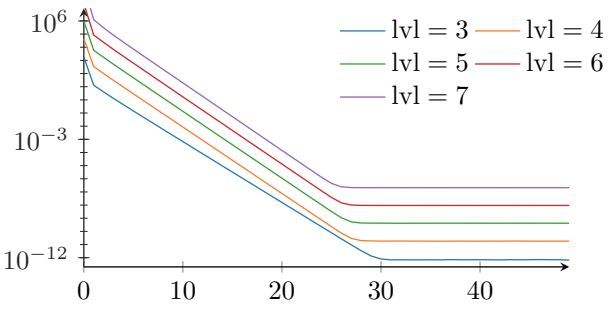

Figure 7: Stokes equations for lid driven cavity: History of norm of residual for multigrid solver employing $\nu = 8$ Richardson smoothing steps with Jacobi preconditioning and full coarse grid correction.

By increasing the number of smoothing steps, the rate of convergence improves and less iterations are required to reach a desired stopping criterion (cf. Table 4). However, the use of more smoothing steps does not necessarily reduce the total computational time, because each multigrid iteration becomes more expensive. Instead, the convergence behavior can be improved without substantial additional effort by utilizing the adaptive coarse grid correction. Especially for $\nu = 8$ smoothing steps, each iteration of the multigrid algorithm using the step length control results in a similar convergence behavior as two iterations of the method employing $\alpha_t = 1$. Another improvement can be achieved by using Gauß-Seidel preconditioning. The application of this preconditioner is obviously more expensive, but the rate of convergence improves nearly for all choices of ν and mesh levels lvl.

4.2 Flow around cube

The next test case is given by the *flow around cube* problem, where the domain $\Omega = (0, 2.5) \times (0, 0.41)^2 \setminus [0.45, 0.55] \times [0.15, 0.25]^2$ is decomposed into $19 \cdot 3^2 - 1 = 170$ cuboidal cells on the coarsest mesh level (cf. Fig. 6a). Here and in all subsequent test problems, a vanishing external force $\mathbf{h}$ is acting on the fluid on the Neumann boundary part Γ_N of the domain specified by

$$\Gamma_N = \left\{ \mathbf{s} \in \partial\Omega : \mathbf{n}_\Omega = (1, 0, 0)^\top \right\}. \tag{12}$$

Furthermore, we always enforce a parabolic inflow boundary profile

$$\mathbf{v}_D(\mathbf{x}) = \begin{pmatrix} 1 \\ 0 \\ 0 \end{pmatrix} u_{\max} \frac{4x_2(0.41 - x_2)}{0.41^2} \frac{4x_3(0.41 - x_3)}{0.41^2}, \quad u_{\max} = 0.45$$

on $\Gamma_{in} = \{0\} \times (0, 0.41)^2$ and prescribe wall boundary conditions $\mathbf{v}_D = \mathbf{0}$ on the remaining boundary part $\partial\Omega \setminus (\Gamma_N \cup \Gamma_{in})$. Finally, the viscosity parameter is set to $\nu = 0.001$ for the incompressible Stokes equations under investigation.

In this problem, the computational domain contains a hole and the Dirichlet boundary part is a union of two separated boundary parts. These parts can be treated independently when applying Dirichlet boundary conditions and do not significantly affect the rate of convergence

Table 4: Stokes equations for lid driven cavity: Experimental rate of convergence for multigrid algorithm employing Richardson smoother.

		full coarse grid correction			adaptive coarse grid correction		
		$\nu = 4$	$\nu = 8$	$\nu = 16$	$\nu = 4$	$\nu = 8$	$\nu = 16$
Jacobi	lvl $= 3$	0.437	0.346	0.262	0.276	0.168	0.164
	lvl $= 4$	0.386	0.313	0.251	0.311	0.101	0.099
	lvl $= 5$	0.383	0.311	0.250	0.312	0.125	0.127
	lvl $= 6$	0.380	0.309	0.249	0.315	0.109	0.108
	lvl $= 7$	0.378	0.307	0.248	0.316	0.105	0.114
Gauß-Seidel	lvl $= 3$	0.273	0.207	0.136	0.191	0.162	0.111
	lvl $= 4$	0.259	0.204	0.158	0.115	0.110	0.108
	lvl $= 5$	0.259	0.204	0.156	0.129	0.097	0.045
	lvl $= 6$	0.258	0.203	0.156	0.106	0.110	0.059
	lvl $= 7$	0.257	0.203	0.155	0.140	0.080	0.048

(cf. Table 5). While the value of ϱ slightly deteriorates on finer meshes for $\nu = 4$ iterations of the Richardson smoother and Jacobi preconditioning, the solution procedure even improves for higher mesh resolutions when employing the Gauß-Seidel preconditioner. On the other hand, performing more than $\nu = 8$ or $\nu = 4$ smoothing steps only slightly reduces the experimental rate of convergence ϱ for Jacobi or Gauß-Seidel preconditioning, respectively. For the latter preconditioner, even the use of a GMRES smoother automatically determining 'optimal' relaxation parameters only pays off on coarser mesh levels for many smoothing steps. On the other hand, the use of this smoothing strategy drastically accelerates the convergence of the multigrid algorithm for a few smoothing steps in case of Jacobi preconditioning.

4.3 Flow around cylinder

The three-dimensional *flow around cylinder* benchmark was originally proposed by Schäfer et al. [Sch+96] and simulates the flow of an incompressible and viscous fluid around a cylindrical obstacle $\Omega_{\text{ob}} = \left\{(x, y, z)^\top \in \mathbb{R}^3 : (x - 0.5)^2 + (y - 0.2)^2 < 0.05^2\right\}$. For this test case, the domain reads $\Omega = (0, 2.5) \times (0, 0.41)^2 \setminus \overline{\Omega_{\text{ob}}}$ (cf. Fig. 6b), while the boundary conditions are defined as introduced in Section 4.2. Furthermore, in the refinement process, the boundary of the unstructured mesh is adapted near the obstacle to accurately approximate its cylindrical surface. Note that Algorithm 1 does not cover the construction of a basis for this doughnut-shaped geometry and more sophisticated strategies are necessary to satisfy all requirements formulated in Sections 2.2 and 2.3. Additionally, a 'global' function has to be introduced to determine the correct net fluxes on both sides of the obstacle. All these aspects slightly hinder the convergence behavior of the multigrid algorithm and justify the use of a few additional smoothing steps (cf. Table 6). However, good convergence behaviors can already be observed for a few smoothing steps and the Gauß-Seidel preconditioner. For $\nu = 4$ GMRES iterations, a single iteration of this multigrid algorithm reduces the norm of

Table 5: Stokes equations for flow around cube: Experimental rate of convergence for multigrid algorithm employing adaptive coarse grid correction.

		Richardson			GMRES		
		$\nu = 4$	$\nu = 8$	$\nu = 16$	$\nu = 4$	$\nu = 8$	$\nu = 16$
Jacobi	lvl $= 1$	0.325	0.220	0.225	0.228	0.177	0.033
	lvl $= 2$	0.363	0.157	0.125	0.131	0.139	0.152
	lvl $= 3$	0.436	0.183	0.078	0.105	0.055	0.049
	lvl $= 4$	0.449	0.170	0.078	0.113	0.063	0.037
Gauß-Seid.	lvl $= 1$	0.241	0.213	0.155	0.166	0.034	0.001
	lvl $= 2$	0.142	0.141	0.145	0.150	0.155	0.083
	lvl $= 3$	0.086	0.060	0.051	0.058	0.053	0.056
	lvl $= 4$	0.085	0.064	0.041	0.059	0.034	0.031

Table 6: Flow around cylinder: Experimental rate of convergence for multigrid algorithm employing GMRES smoother and adaptive coarse grid correction.

		Stokes				Oseen			
		$\nu = 4$	$\nu = 8$	$\nu = 16$	$\nu = 32$	$\nu = 4$	$\nu = 8$	$\nu = 16$	$\nu = 32$
Jacobi	lvl $= 1$	0.270	0.242	0.250	0.132	0.723	0.505	0.280	0.216
	lvl $= 2$	0.525	0.214	0.135	0.139	0.625	0.732	0.351	0.237
	lvl $= 3$	0.552	0.299	0.088	0.048	0.392	0.220	0.192	0.184
	lvl $= 4$	0.526	0.326	0.167	0.051	0.305	0.206	0.108	0.074
Gauß-Seid.	lvl $= 1$	0.268	0.249	0.110	0.001	0.493	0.247	0.274	0.224
	lvl $= 2$	0.161	0.138	0.141	0.131	0.605	0.266	0.251	0.244
	lvl $= 3$	0.238	0.058	0.047	0.049	0.208	0.192	0.190	0.191
	lvl $= 4$	0.293	0.220	0.094	0.060	0.153	0.087	0.070	0.069

the residual roughly as much as two iterations of the solution strategy employing Jacobi preconditioning.

If the convective term is included in the momentum equation, the Stokes equations are generalized to the Oseen equations, resulting in a Reynolds number of Re = 20. In this case, more multigrid iterations are generally required to reach a desired stopping criterion. This behavior can be particularly observed on coarser mesh levels, where convection plays a more dominant role. As a result, Jacobi preconditioning now becomes competitive for $\nu = 4$ smoothing steps, achieving a similar experimental rate of convergence as for Gauß-Seidel preconditioning. For more smoothing steps, the rate of convergence decreases across all mesh levels and both preconditioning techniques, and the discrepancy between the solution strategies under investigation diminishes.

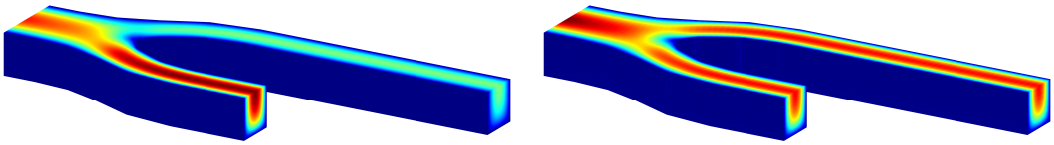

(a) Homogeneous Neumann boundary condition. (b) Flux boundary condition.

Figure 8: Illustration of Stokes solutions for flow through y-pipe using different boundary conditions.

Table 7: Stokes equations for flow through y-pipe: Experimental rate of convergence for multigrid algorithm employing GMRES smoother with Jacobi preconditioning and adaptive coarse grid correction.

	Neumann boundary			Flux boundary		
	$\nu = 4$	$\nu = 8$	$\nu = 16$	$\nu = 4$	$\nu = 8$	$\nu = 16$
$\text{lvl} = 1$	0.184	0.143	0.014	0.148	0.021	0.001
$\text{lvl} = 2$	0.169	0.174	0.195	0.179	0.189	0.084
$\text{lvl} = 3$	0.220	0.134	0.076	0.199	0.114	0.119
$\text{lvl} = 4$	0.241	0.128	0.050	0.246	0.108	0.052

4.4 Flow through y-pipe

Finally, the *flow through a y-pipe* is considered, where the rectangular channel is split into two branches at $x_1 = \frac{41}{72}$, while the upper and lower pipes end at $x_1 = \frac{41}{18}$ and $x_1 = \frac{41}{30}$, respectively (cf. Fig. 6c). Therefore, the Neumann boundary part Γ_{N} defined by (12) is decomposed into two separated segments $\Gamma_{\text{N},1}$ and $\Gamma_{\text{N},2}$ making again the construction of a 'global' function mandatory. For this problem, we either enforce a flux condition splitting the flow into two equally distributed parts or prescribe homogeneous Neumann boundary conditions as mentioned above (cf. Fig. 8). The latter configuration approximately leads to a vanishing pressure variable on both outflow boundary parts, resulting in different pressure drops in the channels and a splitting of the total flux in a ratio of about $2 : 1$. However, the choice of the outflow boundary condition has nearly no impact on the convergence behavior of the multigrid algorithm employing a GMRES smoother with Jacobi preconditioning and the adaptive coarse grid correction (cf. Table 7). Only on coarser meshes and for larger values of ν, the solution procedure converges significantly faster if the flux boundary condition is employed.

In Table 8, we focus on the convergence behavior of the Stokes equations augmented by the reactive term, which can be exploited to investigate the performance of the multigrid solution strategy for time-dependent problems. As expected, the experimental rate of convergence ϱ is in good agreement with the results presented in Table 7 for small values of α and with the adaptive coarse grid correction enabled. As the reactive contribution becomes more

Table 8: Stokes equations for flow through y-pipe using Neumann boundary condition: Experimental rate of convergence for multigrid algorithm employing $\nu = 8$ GMRES smoothing steps with Jacobi preconditioning.

		$\alpha = 10^9$	$\alpha = 10^6$	$\alpha = 10^3$	$\alpha = 1$	$\alpha = 10^{-3}$
full coarse grid correction	lvl = 1	0.023	0.023	0.022	0.057	0.530
	lvl = 2	0.051	0.051	0.049	0.605	0.364
	lvl = 3	0.058	0.058	0.045	0.403	0.297
	lvl = 4	0.053	0.053	0.076	0.333	0.293
adaptive coarse grid correction	lvl = 1	0.063	0.063	0.063	0.023	0.197
	lvl = 2	0.272	0.272	0.270	0.110	0.147
	lvl = 3	0.307	0.307	0.305	0.179	0.109
	lvl = 4	0.304	0.304	0.269	0.088	0.128

dominant, the governing equations converge to the incompressible Darcy equations and the rate of convergence slightly deteriorates, but is still bounded above approximately by 0.3. In this case, the multigrid algorithm performs better when the full coarse grid correction is employed. However, this behavior can only be observed for large values of α and the adaptive coarse grid correction particularly pays off for less dominant reactive contributions.

5 Conclusions

Discretely divergence-free finite elements provide an attractive option for developing solution algorithms for the incompressible Navier-Stokes equations, as they eliminate the need for specialized Schur complement techniques. This makes the approach particularly appealing for problems with high anisotropies in the mesh or differential operators, which require advanced preconditioning strategies. While this methodology has been extensively established in two dimensions, there are only a few references addressing three-dimensional applications. These publications primarily focus on simple geometries without Neumann boundary conditions and ignore the construction of efficient solution techniques per sé.

In this paper, we demonstrate the feasibility of using discretely divergence-free finite elements for more complex and highly resolved three-dimensional problems making the approach practically more relevant. However, this comes with challenges, including the construction of a basis for the coarsest grid level, the development of accurate intergrid transfer operators, and the special handling of boundary conditions. Once these issues are addressed, highly efficient multigrid solvers become available, making this approach particularly attractive for future research.

Open questions are, for example, the design of efficient and robust algorithms for creating a basis. Additionally, a structured and hierarchical method for eliminating certain functions from the spanning set could further reduce the problem size and improve the efficiency of solvers. On the other hand, practical applications may require the use of higher order finite elements. In this regard, the methodology should be extended to other discretization

techniques such as the well-known "Q_2-P_1" finite element pair, which uses continuous, piecewise triquadratic velocity fields with discontinuous, piecewise linear pressure approximations (cf. [BF91]). This extension would not be limited to meshes with planar faces and could potentially lead to even more stable multigrid solvers. Finally, the efficient treatment of time-dependent problems as well as the development of postpressing techniques to recover the pressure unknown in a marching fashion (cf. [GM79; Tur91]) should be considered in order to make this approach competitive with other three-dimensional flow solvers.

Acknowledgements

The author would like to thank Stefan Turek for fruitful discussions and his valuable feedback in the preparation of this paper.

References

[BF91] F. Brezzi and M. Fortin. "Incompressible Materials and Flow Problems". In: *Mixed and Hybrid Finite Element Methods*. Ed. by F. Brezzi and M. Fortin. New York, NY: Springer New York, 1991, pp. 200–273.

[BV90] D. Braess and R. Verfürth. "Multigrid Methods for Nonconforming Finite Element Methods". In: *SIAM Journal on Numerical Analysis* 27.4 (1990), pp. 979–986.

[CR73] M. Crouzeix and P.-A. Raviart. "Conforming and nonconforming finite element methods for solving the stationary Stokes equations I". In: *R.A.I.R.O.* 7 (1973), pp. 33–75.

[Cro76] M. Crouzeix. In: *Proceedings of Journées éléments finis*. Université de Rennes, 1976.

[CSS86] C. Cuvelier, A. Segal, and A. van Steenhoven. *Finite Element Methods and Navier-Stokes Equations*. Dordrecht, Holland: Springer Dordrecht, 1986.

[Dör90] W. Dörfler. "The conditioning of the stiffness matrix for certain elements approximating the incompressibility condition in fluid dynamics". In: *Numerische Mathematik* 58 (1 Dec. 1, 1990), pp. 203–214.

[For81] M. Fortin. "Old and new finite elements for incompressible flows". In: *International Journal for Numerical Methods in Fluids* 1.4 (1981), pp. 347–364.

[GH83] K. Gustafson and R. Hartman. "Divergence-Free Bases for Finite Element Schemes in Hydrodynamics". In: *SIAM Journal on Numerical Analysis* 20.4 (1983), pp. 697–721.

[GM79] D. F. Griffiths and A. R. Mitchell. "Finite elements for incompressible flow". In: *Mathematical Methods in the Applied Sciences* 1.1 (1979), pp. 16–31.

[Gri79] D. F. Griffiths. "The construction of approximately divergence-free finite elements". In: *Proceedings of MAFELAP 1978*. 1979, pp. 237–245.

[Gri81] D. F. Griffiths. "An approximately divergence-free 9-node velocity element (with variations) for incompressible flows". In: *International Journal for Numerical Methods in Fluids* 1.4 (1981), pp. 323–346.

[Hec81] F. Hecht. "Construction d'une base de fonctions P_1 non conforme à divergence nulle dans $\mathbb{R}^3$". fr. In: *RAIRO. Analyse numérique* 15.2 (1981), pp. 119–150.

[HRT96] J. G. Heywood, R. Rannacher, and S. Turek. "Artificial boundaries and flux and pressure conditions for the incompressible Navier–Stokes equations". In: *International Journal for Numerical Methods in Fluids* 22.5 (1996), pp. 325–352.

[KH14] D. Kuzmin and J. Hämäläinen. *Finite Element Methods for Computational Fluid Dynamics: A Practical Guide*. Philadelphia, PA, USA: Society for Industrial and Applied Mathematics, 2014.

[PB87] P. Peisker and D. Braess. "A conjugate gradient method and a multigrid algorithm for Morley s finite element approximation of the biharmonic equation". In: *Numerische Mathematik* 50 (5 Mar. 1, 1987), pp. 567–586.

[RT92] R. Rannacher and S. Turek. "Simple nonconforming quadrilateral Stokes element". In: *Numerical Methods for Partial Differential Equations* 8.2 (1992), pp. 97–111.

[Sch+96] M. Schäfer, S. Turek, F. Durst, E. Krause, and R. Rannacher. "Benchmark computations of laminar flow around a cylinder". In: *Flow simulation with high-performance computers II*. Springer, 1996, pp. 547–566.

[ST94] P. Schreiber and S. Turek. "An efficient finite element solver for the nonstationary incompressible Navier-Stokes equations in two and three dimensions". In: *Numerical methods for the Navier-Stokes equations: Proceedings of the International Workshop Held at Heidelberg, October 25–28, 1993*. Ed. by F.-K. Hebeker, R. Rannacher, and G. Wittum. Wiesbaden: Vieweg+Teubner Verlag, 1994, pp. 268–277.

[Tem77] R. Temam. *Navier–Stokes Equations*. Vol. 2. Studies in Mathematics and Its Applications. Elsevier, 1977.

[Tho81] F. Thomasset. *Implementation of Finite Element Methods for Navier-Stokes Equations*. Berlin, Heidelberg: Springer Berlin Heidelberg, 1981.

[Tur91] S. Turek. "Ein robustes und effizientes Mehrgitterverfahren zur Lösung der instationären, inkompressiblen 2-D Navier-Stokes-Gleichungen mit diskret divergenzfreien finiten Elementen". PhD thesis. Universität Heidelberg, 1991.

[Tur94a] S. Turek. "Multigrid techniques for a divergence-free finite element discretization". In: *East-West Journal of Numerical Mathematics* 2.3 (1994), pp. 229–255.

[Tur94b] S. Turek. "Tools for simulating non-stationary incompressible flow via discretely divergence-free finite element models". In: *International Journal for Numerical Methods in Fluids* 18.1 (1994), pp. 71–105.

[Tur99] S. Turek. *Efficient Solvers for Incompressible Flow Problems: An Algorithmic and Computational Approach*. Berlin, Heidelberg: Springer Berlin Heidelberg, 1999.

[Ver89] R. Verfürth. "On the preconditioning of non-conforming solenoidal finite element approximations of the Stokes equation". In: *Preprint, Universität Zürich* (1989).